**Cell Reports, Volume *34***

## Supplemental information

# Adhesion strength and contractility enable metastatic cells to become adurotactic

**Benjamin Yeoman, Gabriel Shatkin, Pranjali Beri, Afsheen Banisadr, Parag Katira, and Adam J. Engler**

**Supplementary Information**

# Adhesion Strength and Contractility Enable Metastatic Cells to become Adurotactic

Benjamin Yeoman[1,3], Gabriel Shatkin[1], Pranjali Beri,[1] Afsheen Banisadr,[2] Parag Katira[3,4‡], and Adam J. Engler[1,2,5‡]

[1]Department of Bioengineering and [2]Biomedical Sciences Program, University of California, San Diego; La Jolla, CA 92093 USA
[3]Department of Mechanical Engineering and [4]Computational Sciences Research Center, San Diego State University; San Diego, CA 92182 USA
[5]Sanford Consortium for Regenerative Medicine; La Jolla, CA 92037 USA
[‡]Corresponding Authors: pkatira@sdsu.edu
aengler@ucsd.edu

**MANUSCRIPT INFORMATION**

*Abstract Word Count*: 147 words
*Manuscript Word Count*: 28,292 characters (including spaces and figure legends but excluding STAR Methods text, supplemental item legends, and References section)
*Figure Count*: 4
*Supplemental Figure Count*: 4
*Supplemental Video Count*: 7
*Supplemental Tables*: 1

**Running Title**

Weakly Adherent Metastatic Cells are Adurotactic

**Supplemental Figures**

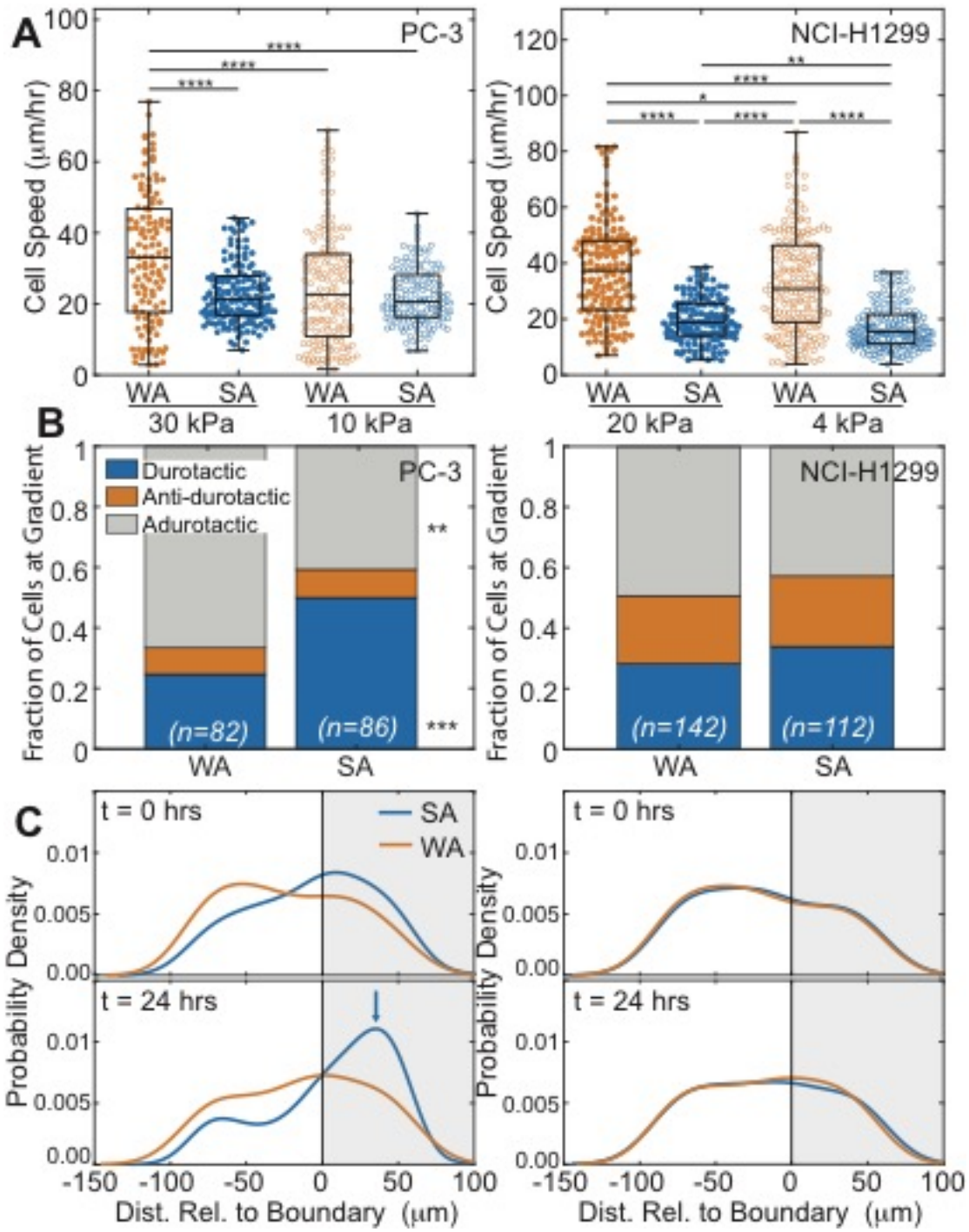


**Supplemental Figure S1: Weakly adherent cells exhibit higher adurotactic behavior, Related to Figure 1. (A)** PC-3 (left) and NCI-H1299 (right) cell speed on soft or stiff side of step-gradient hydrogels is

plotted. Data is shown for cells sorted by adhesion strength, i.e. weakly (orange) vs. strongly (blue), and cells on softer (open) vs. stiffer (closed) regions. (n>200 cells for each condition from triplicate experiments). **(B)** For adhesion sorted PC-3 and NCI-H1299 cells that encounter the step-gradient, the fraction of durotactic, anti-durotactic, and adurotactic behavior is plotted. Data represents n= 82 of 210 WA PC-3 cells and 86 of 246 SA PC-3 cells and n= 142 of 231 WA NCI-H1229 cells and 112 of 247 SA NCI-H1299 cells over triplicate experiments; those not counted did not interact with the gradient. **(C)** At 0 and 24 hours, PC-3 and NCI-H1299 cell probability density versus hydrogel position is shown for weakly (orange) vs. strongly (blue) adherent cells from triplicate experiments. The stiffer region is shaded in gray. Blue arrow indicates a peak in the strongly adherent cell distribution at 24 hours. *p<0.05, **p<$10^{-2}$, ****p<$10^{-4}$, *****p<$10^{-5}$determined by one-way ANOVA with Tukey test for multiple comparisons for the indicated cell speed comparisons and a Fisher's exact for durotactic frequencies for the indicated comparisons.

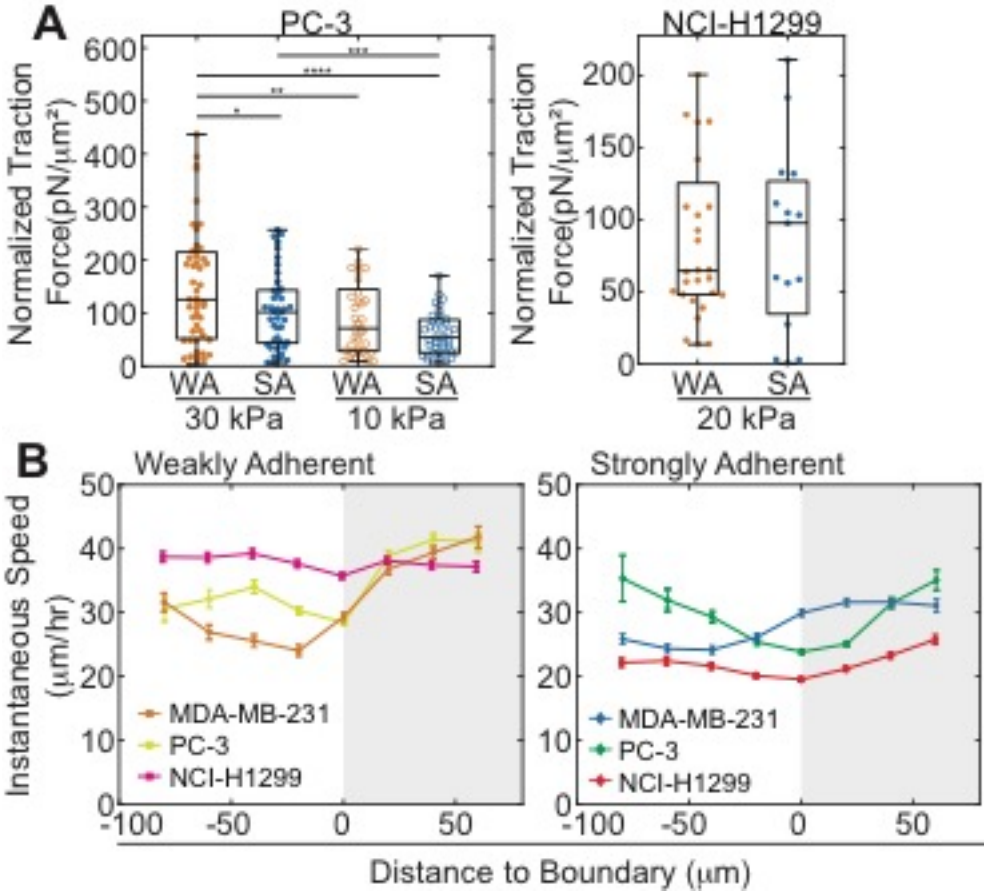


**Supplemental Figure S2: Traction forces and instantaneous speed for PC-3 and NCI-H1299 cells, Related to Figure 2. (A)** Traction force, normalized to cell area, plotted for PC-3 cells on soft or stiff single-modulus (left) hydrogels and NCI-H1299 cells on stiff hydrogels (right). Data is shown for weakly (orange) vs. strongly (blue) adherent cells, and open circles for PC-3 cells on soft (n>47 for PC-3, n>15 for NCI-H1299). *p<0.05, **p<0.01,***p<0.001, and ****p<0.0001 via one-way ANOVA with Tukey test for multiple comparisons for the indicated comparisons. **(B)** Instantaneous cell speed is plotted as a function of position relative to the step-gradient for adhesion sorted weakly (left) and strongly (right) adherent MDA-MB-231 (orange/blue), PC-3 (yellow/green), and NCI-H1299 (pink/red) cells. Negative values are on the soft substrate and positive are on the stiff. Average speed ± standard error of the mean is plotted for n>144 cells for each condition from triplicate experiments.

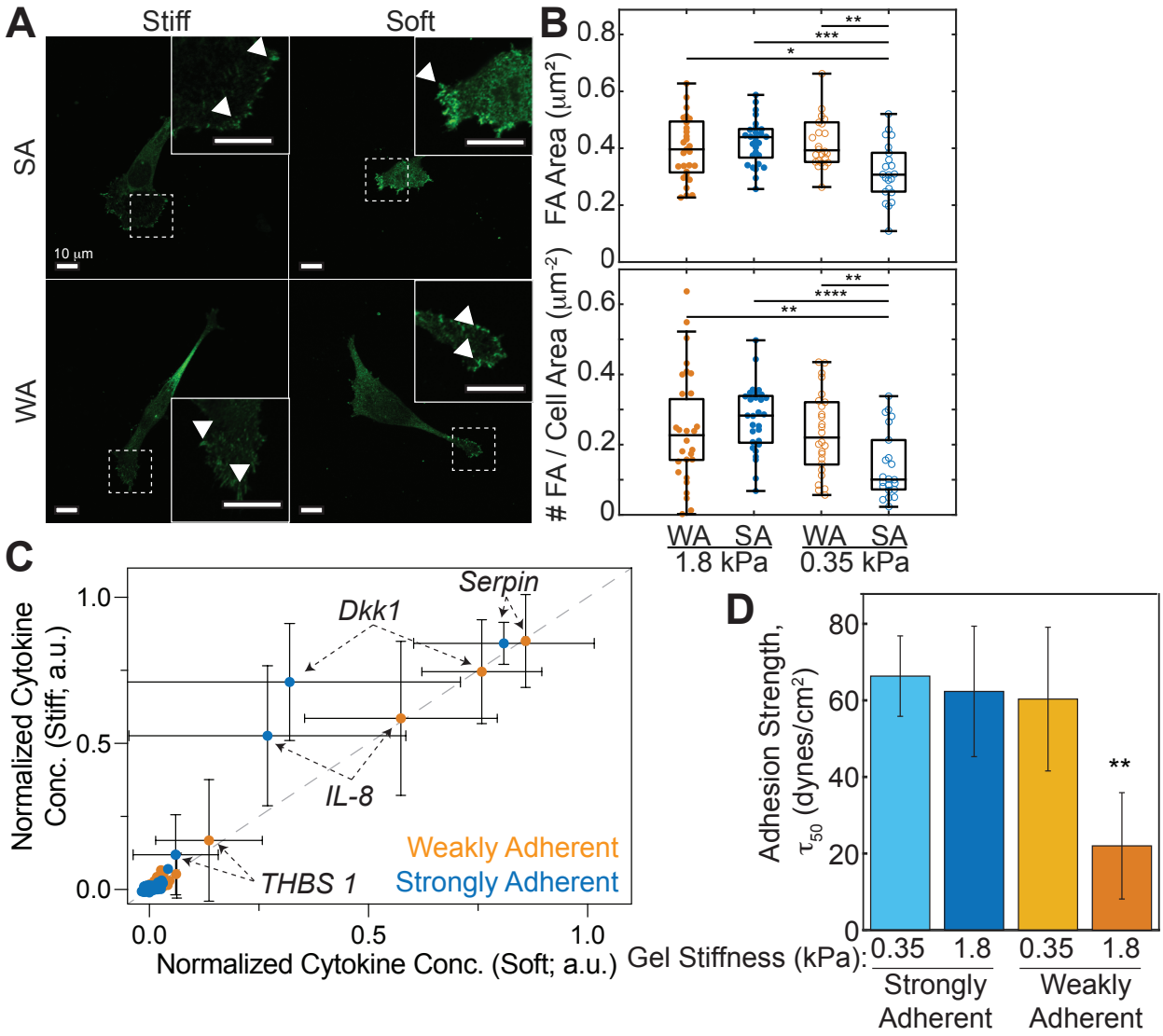


**Supplemental Figure S3: Effects of Focal adhesions, Cytokines, and Stiffness on Adhesion, Related to Figure 2. (A)** Representative images of FAs in weakly and strongly adherent MDA-MB-231 cells on soft or stiff single modulus hydrogels. Paxillin is shown in green and highlighted in the inset images (dashed boxes indicating which regions are magnified) by arrowheads that point to representative paxillin adhesions. Scale bar is 10 μm. **(B)** FA area (top) and number of FAs normalized to cell area (bottom) are plotted for the indicated sorting and elasticities. n>20 cells/condition from triplicate experiments. **(C)** Cytokine expression for WA and SA cells, normalized to loading controls, is plotted ± standard deviation for 105 cytokines found in cell culture media collected from WA (orange) and SA (blue) MDA-MB-231

cells plated onto soft (0.35 kPa) and stiff (1.8 kPa) hydrogels for 24 hours. Specific cytokines expressed above background noise are noted with corresponding error bars from triplicate media collections; dashed arrows link cytokine names with their respective data. No data was statistically different between substrate stiffness or adhesion mechanotype based on one-way ANOVA with Tukey test for multiple comparisons. **(D)** Post-selection weakly and strongly adherent MDA-MB-231 cells were plated onto hydrogels of indicated stiffness and subjected to a shear stress gradient. Adhesion strength or $\tau_{50}$, i.e. the shear stress at which 50% of the population detaches from the substrate, is plotted ± standard deviation. *p<0.05, **p<0.01,***p<0.001, and ****p<0.0001 via one-way ANOVA with Tukey test for multiple comparisons for the indicated comparisons.

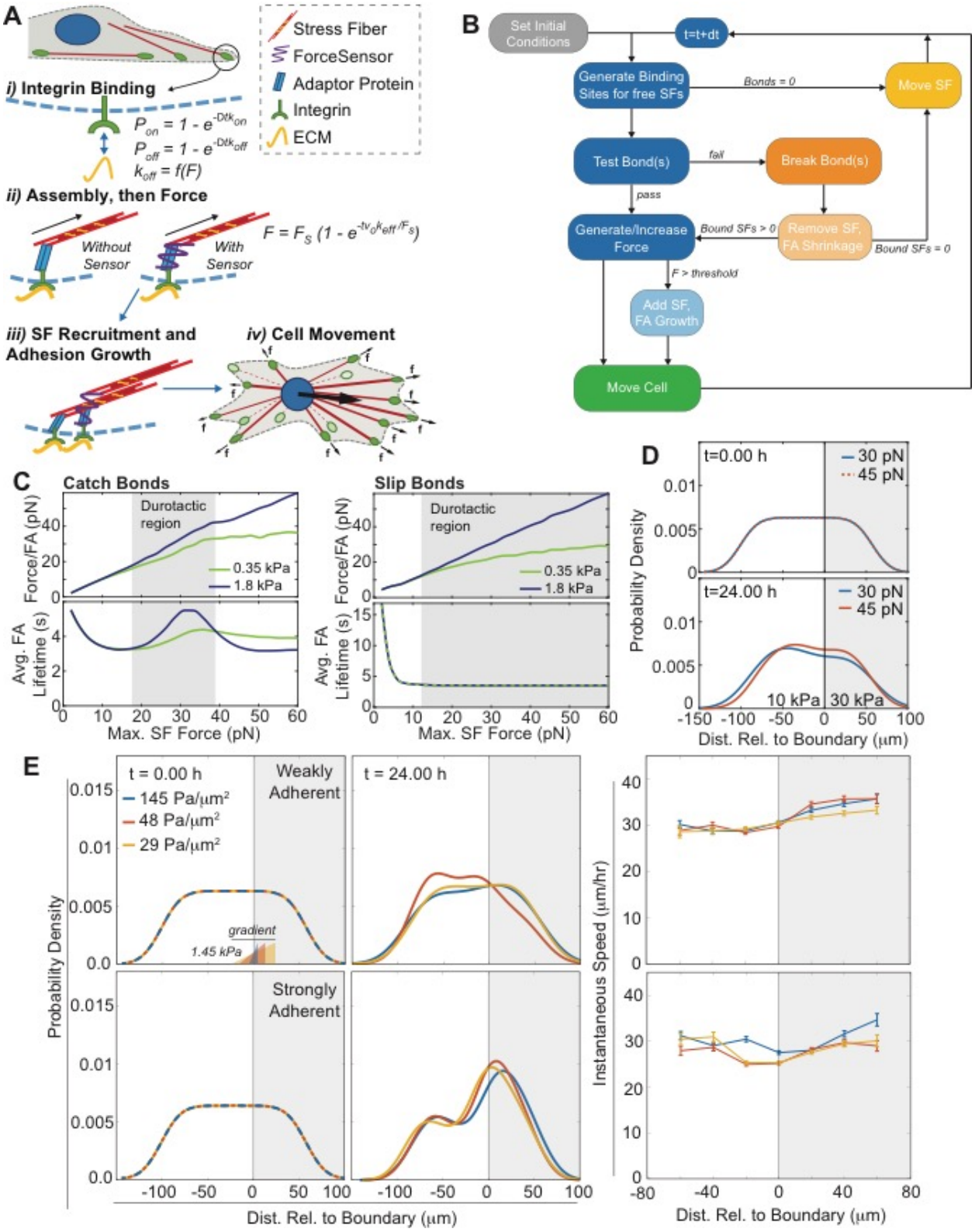


**Supplemental Figure S4: Computational Model Schematic and it's Sensitivity to Stiffness Range and Gradient Strength, Related to Figure 3. (A)** Schematic of rigidity sensing in cells where softer catch

bonds, i.e. strongly adherent cells, leads to asymmetric adhesion maturation at the step-gradient whereas stiffer bonds in weakly adherent cells break and prevent rigidity sensing. This occurs in four phases: i) integrin binding, ii) assembly and force production, iii) adhesion growth and stress fiber recruitment, and iv) cell movement. **(B)** Diagram indicates the decision logic for the computational durotaxis model described in Figures 2 and 3. Gray indicates initial conditions, which feed in to the force on adhesions equations (blue). Adhesion outcomes are shown in orange with cell migration shown in green. Arrows indicate the decision logic with notes about each pathway indicated above or to the side of the decision. **(C)** Comparison of catch (left) and slip (right) bond dynamics, Force/FA (top) and average FA lifetime (bottom) as a function of max SF force for ECM stiffnesses fixed at 0.35 or 1.8 kPa (green and blue, respectively). The gray region highlights where force is greater and bond lifetime is also greater or equal than it is on soft, which corresponds to the onset of durotactic behavior. **(D)** Model cell durotaxis on gradients with a different stiffness range at 0 and 24 hours, model cell probability density versus simulated hydrogel position is shown for cells with 45 pN (orange) vs. 30 pN (blue) max SF force. The stiffer region is shaded in gray (30 kPa) vs. the softer region in white (10 kPa); values were chosen to mirror prostate tumor gradients rather than mammary tumor gradients to which model parameters were otherwise tuned. **(E)** Model cell durotaxis on gradients of different magnitude but same stiffness range**.** (Left) At 0 and 24 hours, model cell probability density versus simulated hydrogel position is shown for cells with 45 pN (Weakly Adherent) vs. 30 pN (Strongly Adherent) max SF force. The stiffer region is shaded in gray (1.8 kPa) vs. the softer region in white (0.35 kPa); gradient slope was changes as indicated. All previous simulations use 145 Pa/$\mu m^2$ (blue) but plots here also include gradients 3- (dark orange) and 5-fold shallower (light orange). (Right) Instantaneous cell velocities ± S.E.M. for the indicated gradients and WA (top) or SA (bottom).

99 **Supplementary Tables**

| Parameter | Description | Value | Source |
|---|---|---|---|
| $\mu_{SF}$ | Average assembly sites/cell | Adjustable, 50 | (Elosegui-Artola et al., 2014) |
| $v_{act\_L}$ | Actin assembly, leading edge | 0.2 μm $s^{-1}$ | (Pollard, 1986; Prahl et al., 2020; Vavylonis et al., 2005) |
| $v_{act\_T}$ | Actin assembly, trailing edge | 0.1 μm $s^{-1}$ | (Pollard, 1986; Prahl et al., 2020; Vavylonis et al., 2005) |
| $v_{ret}$ | Actin disassembly velocity | 0.5 μm $s^{-1}$ | (Vavylonis et al., 2005) |
| $t_{ret}$ | Retraction Time | 10 s | (Bosgraaf and Van Haastert, 2009b, 2009a) |
| $D_{rot}$ | Rotational diffusion constant of F-actin | Calculated, $s^{-1}$ | |
| $k_B$ | Boltzmann's constant | 1.3806E-23 kg $m^2$ $s^{-2}$ $K^{-1}$ | |
| $T$ | Temperature | 310.15 K | |
| $L$ | Length of actin filament | Calculated, μm | |
| $d_{act}$ | Diameter of Actin | 7 nm | (Cooper, 2000) |
| $\eta$ | Cytoplasm (water) viscosity @ 37C | 0.0006913 Pa s | |
| $K_{on}$ | Integrin-SF assembly rate | 0.1 $s^{-1}$ | (Bidone et al., 2019; Vicente-Manzanares et al., 2009) |
| $\mu_{Int}$ | Average Integrins/F-actin | 1 | (Blystone, 2004) |
| $P_{tal}$ | Probability of force-sensor protein | 0.7 | (Himmel et al., 2009) |
| $k_{off}$ | Unbinding rate | Calculated, $s^{-1}$ | |
| $A$ | Fitting constant | 3.309 | |
| $B$ | Fitting constant | 0.0003942 | |
| $C$ | Fitting constant | 58.19 | |
| $\xi$ | Unbinding length | 0.7959 nm | (Kong et al., 2009) |
| $k_0$ | Unloaded off rate | | |
| $F_b$ | Bond rupture force | | |
| $F_S$ | Max filament force | $F_{myo}$ x $n_{myo}$ | |
| $F_{myo}$ | Myosin Motor Force | 2 pN | (Molloy et al., 1995) |
| $n_{myo}$ | # of Myosin Motors/F-actin | Adjustable, 10-25 | (Cooper and Hausman, 2007) |
| $v_0$ | Myosin sliding velocity | 1 μm $s^{-1}$ | (Brizendine et al., 2015) |
| $K_{ECM}$ | ECM stiffness | ECM modulus x 0.1 μm | length scale typical for myosin sensing |
| $E_{stiff}$ | Young's modulus, Stiff | 1800 Pa, Measured experimentally | |
| $E_{soft}$ | Young's modulus, Soft | 350 Pa, Measured experimentally | |
| $L_{grad}$ | Gradient Length | 10 μm, from AFM measurements | |
| $F_{thres}$ | Force sensor threshold | 1 pN | (Grashoff et al., 2010; Rio et al., 2009) |
| $K_{act}$ | Actin-Talin assembly rate | 1 $s^{-1}$ | (Tapia-Rojo et al., 2020) |
| $n_{SF}$ | Maximum SFs/FA | Adjustable, 100 | (Prahl et al., 2020) |
| $\Pi$ | Bond friction factor | $2 \times 10^{-5}$ kg $s^{-1}$ | (Pompe et al., 2011) |

**Supplementary Table S1: Model parameters for the cell durotaxis model, Related to STAR Methods.**

Parameters are listed in order of appearance in methods section. Note that for Figure S7, $E_{stiff}$ and $E_{soft}$ were changed as indicated.